Influence of gallium ion beam acceleration voltage on the bend angle of amorphous silicon cantilevers

2016 Jpn. J. Appl. Phys. 55 06GL02

(http://iopscience.iop.org/1347-4065/55/6S1/06GL02)

Japanese Journal of Applied Physics **55**, 06GL02 (2016)
http://doi.org/10.7567/JJAP.55.06GL02

REGULAR PAPER

Influence of gallium ion beam acceleration voltage on the bend angle of amorphous silicon cantilevers

Takahiro Kozeki[1], Hoang-Phuong Phan[2], Dzung Viet Dao[2,3], Shozo Inoue[1], and Takahiro Namazu[1*]

[1]*Department of Mechanical Engineering, University of Hyogo, Himeji, Hyogo 671-2201, Japan*
[2]*Queensland Micro-Nanotechnology Centre, Griffith University, Nathan, Qld 4111, Australia*
[3]*School of Engineering, Griffith University, Nathan, Qld 4111, Australia*

*E-mail: namazu@eng.u-hyogo.ac.jp

Received December 8, 2015; revised March 3, 2016; accepted March 9, 2016; published online May 11, 2016

This paper describes a plastic reshaping technique for Si thin membranes by using focused ion beam (FIB) processing. FIB is used to locally pattern and implant Ga ions into the membranes. The combination of Ga ion doping and alkali wet etching enables us to fabricate nanometer-thick Ga-ion-doped amorphous Si membranes, which can be bent upward at arbitrary angle by controlling the FIB beam irradiation condition. The bending mechanism is discussed in the light of Ga ions implanted depth from the membrane surface. By using this technique, a micrometer-sized chute structure with several different angles is produced.

1. Introduction

Semiconductor fabrication technologies play the important roles for the miniaturization of electronic devices and microelectromechanical systems (MEMS), which contribute the development of various compact, portable and multi-functional applications.[1,2] Among many semiconductor materials used in MEMS, Si is the first choice material owning to its worldwide availability, mature fabrication process, and various excellent physical properties.[3–6] Due to its brittleness, Si cannot be deformed plastically within the range from room temperature to intermediate temperature, which restricts the availability as the structural material for three-dimensional (3D) MEMS.[7–12] Si nano-membrane is the attractive material for nanomechanical elements, which can be used for nano force sensors, pressure sensors, acoustic sensors, and nano oscillators in nanoelectromechanical systems (NEMS).[13–18] If the membrane can be deformed freely to 3D arbitral shape, high-performance and highly-integrated 3D Si MEMS and NEMS devices will be realized hopefully. An ion implantation technique with Ar ion beam is one of the unique methods for deforming thin films into a vertically-bent 3D shape. In the case of a thin film cantilever beam, the radius of curvature in the out-of-plane direction can be controlled.[19,20] However, owing to its entire irradiation, a thin film cantilever cannot be bent locally and sharply. This will restrict its application to MEMS and NEMS devices.

Focused ion beam (FIB) is well known as a powerful tool for directly forming micro/nano-scale 3D mechanical structures without photolithography.[21] A damaged layer is always produced on the fabricated sample surface, but the FIB technique can be also used as an ion implantation tool under low beam current condition. In this technique, a thin membrane can be reshaped freely and finely because the ion beam is focused. In addition, the FIB technique can be employed to amorphize a Si film, which enables us to fabricate released/suspended Si nano thin membranes due to the low etching rate of amorphous Si with respect to single crystalline Si.[22–26]

In this study, we describe a novel technique to create 3D nano structures made from 2D Si nano membranes by using FIB. Amorphous Si cantilever beams are produced by combining FIB ion implantation and ion-doped selective wet etching techniques. The beams are deformed locally in the out-of-plane direction by using local FIB irradiation. The relationship between FIB irradiation depth and bent angle is investigated. By using the local FIB irradiation technique, 3D MEMS structure like a chute with several different angles is successfully produced.

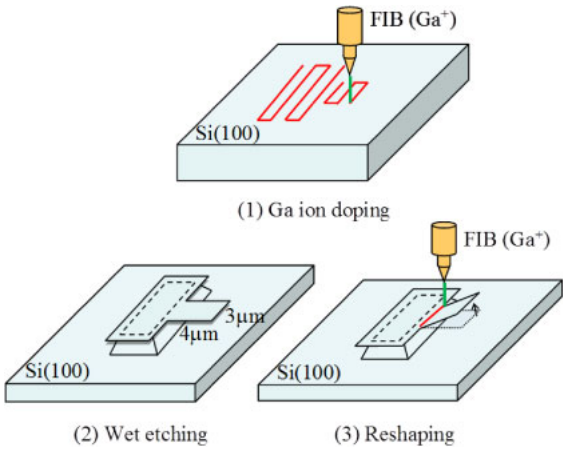

Fig. 1. (Color online) Schematic of fabrication process for nanometer-thick Si cantilever with FIB and wet etching along with a schematic of the bending with local FIB irradiation.

2. Fabrication of Si nano cantilevers

Figure 1 illustrates the process flow for fabricating a silicon nano membrane and reshaping it by localized Ga ion implantation. First, Ga ion was irradiated in the shape of a Si cantilever on a Si(100) surface with an ion dose 7×10^{15} ions/cm^2 and an accelerating voltage of 40 kV. The samples were then etched in 20% aqueous tetramethyl-ammonium hydroxide (TMAH) solution at 90 °C. The localized Ga ion implantation portion remained after wet etching, and subsequently the cantilevers were released from the substrate as a result of Si under etching. We also observed that the cantilevers lied on the same plane as the Si original film, indicating that there was no residual stress after wet etching. Finally, by irradiating Ga ion beam in the vicinity of the cantilever fixed end, the cantilever can be bent in response to the implantation condition. The amount of doses

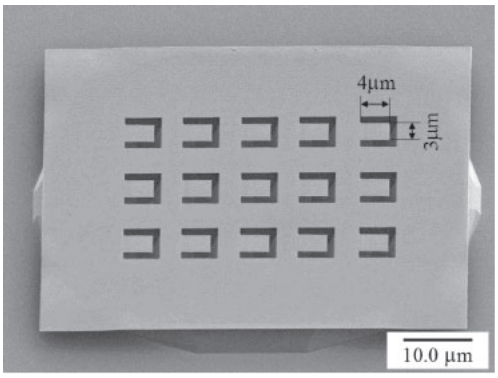

Fig. 2. SEM image of Si nano-cantilever array. $3 \times 4\,\mu m^2$ Si cantilevers were fabricated simultaneously by FIB irradiation and wet etching.

per scan was set to be from 9.0×10^{13} to 1.8×10^{14}. This experiment was conducted using commercial FIB apparatus (Hitachi High Technologies: FB2200). Figure 2 shows an array of 3×5 standing Si cantilevers fabricated using the above-mentioned method. The dimensions of these cantilevers were $4 \times 3 \times 0.06\,\mu m^3$, in which the thickness was estimated based on scanning electron microscope (SEM) images observed when tilting the samples. Under these conditions, the (100) planes appear in parallel to the direction of the cantilevers, and no residual stress affecting cantilever bending was detected. The fixed end of the cantilevers was undercut by etching and the undercut sidewall was composed of Si(111) surface due to anisotropic etching with TMAH.

Figures 3(a)–3(f) show the representative SEM images of 40-kV-formed Si thin cantilevers bent by Ga ion doping at 40, 30, 20, 10, 5, and 2 kV, respectively. The beam current was set at very low value of approximately 0.03 nA. The digits written in these figures are indicative of the number of the ion beam scan cycles. In Ga ion beam scanning at 40 kV and 0.01 nA, as shown in Fig. 3(a), the cantilevers are found to be gradually bent upward when increasing the number of the beam scan cycles. The maximum bend angle was approximately 90°, which was obtained after 45 cycles scanning. At 30 kV in Fig. 3(b), the cantilevers at the top row of the sample have noticeably different bending angles because of the high beam current, 0.07 nA, whereas the cantilevers at the second row have smaller bending angles owning to their low beam current, 0.01 nA. Owing to the same current value, the angles of each cantilever in the scan cycles from 5 to 45 look similar to those at 40 kV. At 20 kV and 0.02 nA shown in Fig. 3(c), the relation between the scan cycles and angle was almost similar to those at 40 and 30 kV scanning, although it is obvious that the deformation angle of the cantilever after 10 cycles was much smaller than that of the cantilevers at the same cycles in higher voltages due to the influence of the dust on the cantilever. However, at 10 kV and 0.02 nA in Fig. 3(d), we could observe a phenomenon different from the previous samples shown in Figs. 3(a)–3(c). That is, the cantilevers were bent upward by irradiating Ga ions locally, but the angles were smaller than those in the cantilevers bent at higher voltages. Moreover, at a number of scan cycles above 70, the bending angle reached its saturated state, and did not change any more even when increasing scan cycles. In Fig. 3(e), the beam current used this time was 0.06 nA, slightly higher than the previous experiments because the acceleration voltage was extremely low. In this case, for scan cycles below 100, we found that the color and the thickness of the root part of the cantilevers changed, while no significant bending angle was observed. However, at larger scan cycles, the cantilevers were rapidly bent upward, with their bending angle reaching nearly 90°. In Fig. 3(f), the cantilevers were only slightly bent upward even at a high scan cycle of 200, and no rapid increase in the bending angle was observed.

From these results, after irradiating Ga ions, we found that all the cantilevers were bent upwards, and the magnitude of the deflection increased with increasing the number of beam scan cycles. Additionally, the tendency of deformation of the cantilevers significantly depended on the applied accelerating voltage.

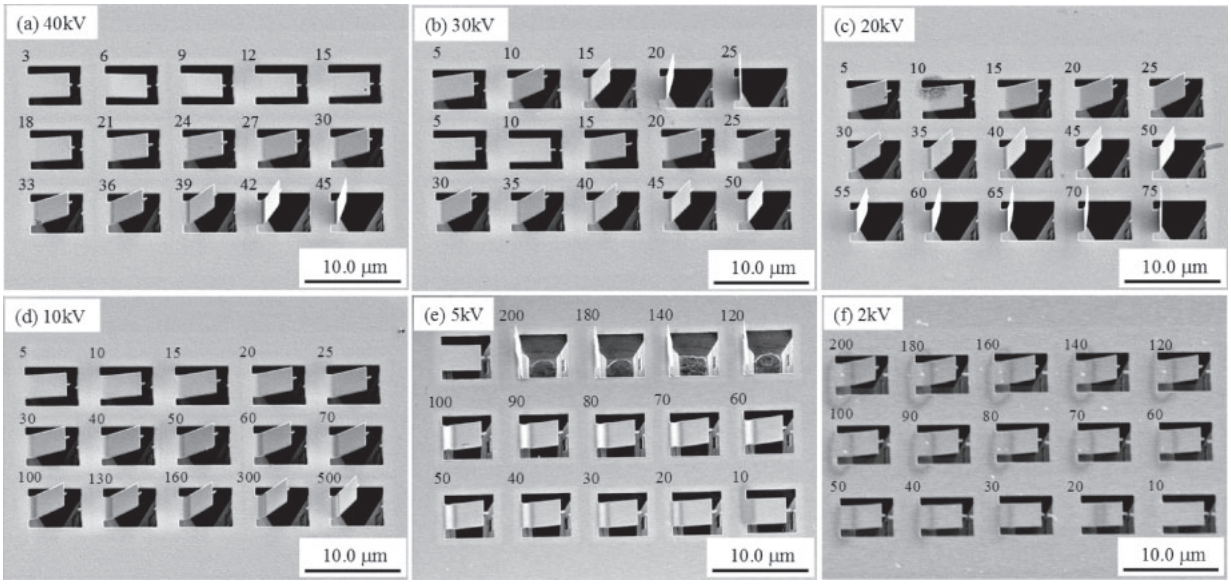

Fig. 3. SEM photographs of bent cantilevers by FIB with the accelerating voltage of 2 to 40 kV. The bend angles are found to strongly depend on the accelerating voltage in FIB implantation.

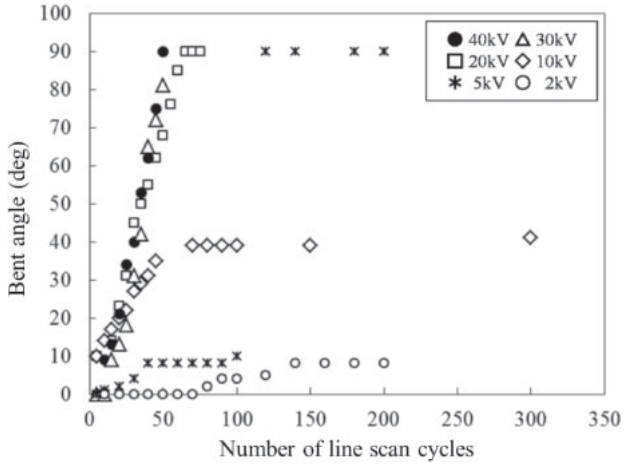

Fig. 4. Relationship between the number of line scan cycles for cantilever bending and the bend angle.

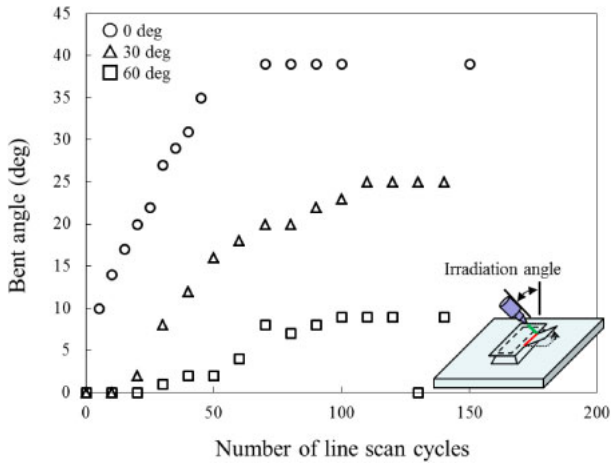

Fig. 5. (Color online) Relationship between FIB irradiation angle and the bend angle.

3. Deformation angle and mechanism

Figure 4 presents the relationship between the number of scan cycles and the bend angle of the 40-kV-formed cantilevers. At the accelerating voltage of 2 kV, the cantilevers did not deform so much. Even after 200 cycles, the angle was approximately 10° at the maximum. At 5 kV, when scan cycles were less than 100 kV, the maximum bent angle was around 10°. However, after 120 cycles, the cantilevers were abruptly bent to 90°. At 10 kV, the bend angle of cantilevers increased to 40° with increasing the number of scan cycles to 50 cycles. The angle increasing rate can be estimated to be 0.77°/cycle, which is 17.5 and 3.85 times faster than those at 2 and 5 kV. Over 50 cycles, however, the bend angle was stayed constant at around 40°. In the case of the voltage over 20 kV, a similar trend can be seen. The angle increasing rate was 1.36°/cycle, which is 1.77 times faster than that at 10 kV. At around 50 cycles, the angle reached the maximum angle of 90°.

Figure 5 shows the relationship between the number of line scan angles and bent angle when Ga ion beam was irradiated from different angles. The beam angles were set to be 0, 30, and 60° from the normal direction of the cantilevers. All the cantilevers were formed at 40 kV and were bent at 10 kV. At the irradiation angle of 0°, the cantilever was bent upward. The relation between the scan cycles and bent angle is almost linear below 50 cycles. The deformation rate was 0.7°/cycle. In greater cycles, the angle was saturated at around 40°. With increasing the irradiation angle, the deformation rate decreases. At 60°, the deformation rate was 0.1°/cycle. The maximum deformation angles were approximately 26 and 8° at the irradiation angles of 30 and 60°, respectively. Since the penetration depth of Ga ions is known to depend on the irradiation angle, it is found that the deformation of the cantilevers is related to the penetration depth.

We analyzed the distribution of 10,000 Ga ions vertically irradiated at 40 kV to the Si surface by using ion impact analysis software with the Monte Carlo simulation, the SRIM.[27] By using the results, the bending mechanism is illustrated in Fig. 6. Although the SRIM data are not presented here, the analyses implied that the density of doped Ga ions in the Si cantilever is nonuniform along the thickness direction. The compressive stress is known to be generated in an ion doped material,[28,29] which indicates that the cantilever is deformed by the slope of compression stress originating from ion distribution. The implanted depth of Ga ions depended on the accelerating voltage.[30] When the voltage was 5 kV, the maximum penetration depth and Ga ions density peak position from the surface can be estimated to be 20 and 9 nm, respectively, in the case of single crystal Si. Although the peak position of doped Ga ions was closer to the top surface from the neutral axis of the cantilever, the cantilever was bent upward slightly. This would be caused by the difference between single crystal Si and amorphous Si used in the SRIM analysis and the experiments, respectively. Since amorphous Si is softer than single crystal Si, Ga ions would have been penetrated into deeper portion than expected. From the fact that the bend angle was very small, the peak position is supposed to be in the vicinity of the neutral axis. When the voltage increased to 40 kV, the peak position of implanted Ga ions was approximately 35 nm from the top surface. This value was obtained based on the assumption that the sample was single crystal Si, so the actual peak position can be estimated to be closer to the backside of the cantilever; consequently the cantilever was bent upward rapidly due to strong compressive stress generated in the vicinity of the backside of the cantilever. However, even at 5 kV, the long time Ga ions irradiation provides a large upward bending with the cantilever. By successive Ga ions irradiation, Ga ions were accumulated in the middle of the cantilever. At the same time, Si atoms around the top surface were sputtered gradually; consequently, the irradiated portion was thinned and deformed as shown in the SEM image in Fig. 6. Therefore, the Ga ions accumulation and Si sputtering would have caused a large deformation of Si cantilevers.

4. Application

To demonstrate the availability of the experimental data indicating the relationship between the number of scan cycles and bent angle, a chute-like structure was fabricated as shown in Fig. 7. First, a development elevation pattern of a chute made of amorphous Si was fabricated by the combination of FIB implantation and selective wet etching techniques. Then, the guardrails were bent by irradiating FIB under the accelerating voltage and the number of scan cycles of

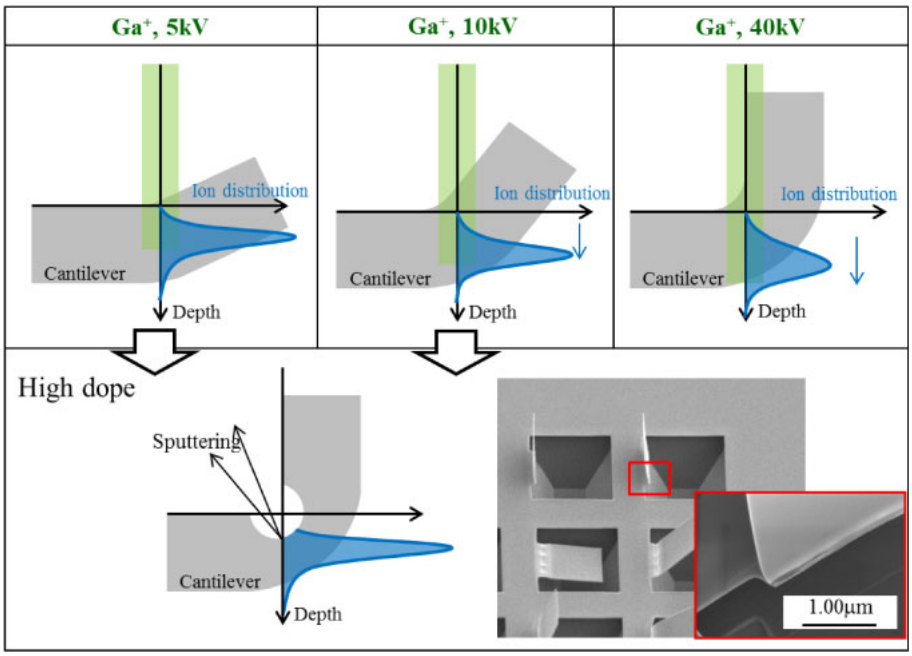

Fig. 6. (Color online) Schematic of the deformation mechanism of Si nano cantilevers by FIB.

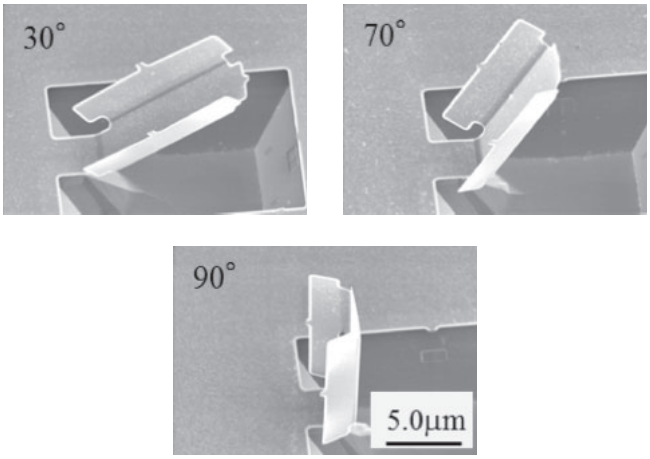

Fig. 7. SEM images of produced Si chute by local FIB irradiation technique.

40 kV and 60 cycles, respectively. After that, the fixed end of the chute was bent at 40 kV and 20 cycles. The bent angle was approximately 30°, which was identical to the experimental data base shown in Fig. 4. With increasing the cycles to 40 and 60 cycles, the angle increased to 70 and 90°. By using the local FIB irradiation technique, we demonstrated that 3D arbitral mechanical structures made of amorphous Si can be made.

5. Conclusions

We proposed a method for manufacturing 3D Si structures using FIB. Si nano cantilevers were fabricated by means of Ga ion implantation by FIB and wet etching by TMAH. Si thin film was locally amorphized using Ga ion implantation, which enabled us to fabricate released nanometer-thick cantilevers due to selective Si etching. By irradiating Ga ion beam into the fixed end only, the cantilever could be bent in response to the irradiation condition. The experimental results showed that the bend angle of standing cantilevers remarkable depended on the acceleration voltage. Under low acceleration voltages of below 10 kV, the bend angle reached a saturated value of below 40° even when increasing the scan cycles; however under higher voltage (e.g., 40 kV), cantilevers could be bent upward at an angle of approximately 90°. We assumed that the stress induced by the penetration of Ga ions into the deep portion of Si cantilevers was the origin of this bending phenomenon. We successfully fabricated 3D mechanical structure like a chute by using adequate accelerating voltage and line scan cycles in FIB irradiation. The bending technique proposed in this work would be expected to be applicable in fabricating more complex 3D structures.

1) H.-P. Phan, D. V. Dao, K. Nakamura, S. Dimitrijev, and N.-T. Nguyen, J. Microelectromech. Syst. **24**, 1663 (2015).
2) H.-P. Phan, T. Kozeki, T. Dinh, A. Qamar, Y. Zhu, T. Namazu, N.-T. Nguyen, and D. V. Dao, RSC Adv. **5**, 82121 (2015).
3) A. A. G. Requicha, Proc. IEEE **91**, 1922 (2003).
4) J. Verd, G. Abadal, J. Teva, M. V. Gaudo, A. Uranga, X. Borrise, F. Campabadal, J. Esteve, E. F. Costa, F. Perez-Murano, Z. J. Davis, E. Forsen, A. Boisen, and N. Barniol, J. Microelectromech. Syst. **14**, 508 (2005).
5) D. Chiba, S. Fukami, K. Shimamura, N. Ishiwata, K. Kobayashi, and T. Ono, Nat. Mater. **10**, 853 (2011).
6) H. Fujita, *Micro-Nanomasin Gijutsu Nyumon* (Kogyo Chosakai, Tokyo, 2003) [in Japanese].
7) A. Luque, J. M. Moreno, J. Brey, C. D. Ellis, J. M. Quero, and B. M. Wilamowski, J. Microelectromech. Syst. **19**, 384 (2010).
8) M. Mehregany, C. A. Zorman, N. Rajan, and H. W. Chien, Proc. IEEE **86**, 1594 (1998).
9) T. Namazu, Y. Tashiro, and S. Inoue, J. Micromech. Microeng. **17**, 154 (2007).
10) O. Tabata, R. Asahi, H. Funabashi, K. Shimaoka, and S. Sugiyama, Sens. Actuators A **34**, 51 (1992).
11) M. Shikida, T. Hasada, and K. Sato, J. Micromech. Microeng. **16**, 1740 (2006).
12) M. J. de Boer, J. G. E. Gardeniers, H. V. Jansen, E. Smulders, M.-J. Gilde, G. Roelofs, J. N. Sasserath, and M. Elwenspoek, J. Microelectromech. Syst. **11**, 385 (2002).

13) A. J. Steckl, H. C. Mogul, and S. Mogren, Appl. Phys. Lett. **60**, 1833 (1992).
14) D. R. Miranda, R. Moreno, and G. Iapochonp, Intensive Care Med. **23**, 760 (1997).
15) N. Kacem, J. Arcamone, F. P. Murano, and S. Hentz, J. Micromech. Microeng. **20**, 045023 (2010).
16) K. L. Ekinci and M. L. Roukes, Rev. Sci. Instrum. **76**, 061101 (2005).
17) K. T. Lam, C. Lee, and G. Liang, Appl. Phys. Lett. **95**, 143107 (2009).
18) A. Koochi, A. Farrokhabadi, and M. Abadyan, Microsyst. Technol. **21**, 355 (2015).
19) T. Yoshida, M. Nagao, and S. Kanemaru, Appl. Phys. Express **2**, 066501 (2009).
20) T. Yoshida, M. Nagao, A. Baba, T. Asano, and S. Kanemaru, J. Vac. Sci. Technol. **27**, 729 (2009).
21) T. Fujii, T. Namazu, K. Sudoh, S. Sakakihara, and S. Inoue, J. Eng. Mater. Technol. **135**, 041002 (2013).
22) P. Sievilä, N. Chekurov, and I. Tittonen, Nanotechnology **21**, 145301 (2010).
23) N. Chekurov, K. Gropras, A. Peltonen, S. Franssila, and I. Tittonen, Nanotechnology **20**, 065307 (2009).
24) I. L. Berry and A. L. Caviglia, J. Vac. Sci. Technol. **1**, 1059 (1983).
25) A. J. Steckl, H. C. Mogren, and S. Mogren, Appl. Phys. Lett. **60**, 1833 (1992).
26) N. Kawasegi, N. Morita, S. Yamada, N. Takano, T. Oyama, K. Ashida, J. Taniguchi, and I. Miyamoto, JSME Int. J., Ser. C **49**, 583 (2006).
27) J. F. Ziegler, M. D. Ziegler, and J. P. Biersack, Nucl. Instrum. Methods Phys. Res., Sect. B **268**, 1818 (2010).
28) D. R. McKenzie, J. Vac. Sci. Technol. **11**, 1928 (1993).
29) N. E. W. Hartley, J. Vac. Sci. Technol. **12**, 485 (1975).
30) JEOL Application Data Sheet IB-A-004-00.